Astron. Astrophys. 189, 263–276 (1988)

ASTRONOMY AND ASTROPHYSICS

Velocity and temperature in solar magnetic fluxtubes from a statistical centre-to-limb analysis

F.G.E. Pantellini, S.K. Solanki, and J.O. Stenflo

Institute of Astronomy, ETH-Zentrum, CH-8092 Zürich, Switzerland

Received July 7, accepted July 22, 1987

Summary: A statistical analysis of Stokes I and V profiles of a large number of unblended Fe I lines, which have been observed at different positions on the solar disk, is carried out. The centre to limb variation (CLV) of various parameters of the line profiles formed inside the fluxtubes is analysed. The dependences of some of these parameters on filling factor and on μ are partially separated using regression equations. The asymmetry of the Stokes V profile is studied in great detail. In particular, the change of its sign when approaching the limb, previously observed for a few medium strong lines, is established for a significantly broader sample. The detailed CLV of the area asymmetry is however found to be strongly dependent on line strength. The CLV of the zero-crossing wavelength of the weak and medium strong lines is compatible with the absence of stationary flows in fluxtubes. At all limb distances the stronger lines are more blueshifted than the weak ones. Model calculations are carried out and the temperature models of solar magnetic fluxtubes of Solanki (1986) are tested. They are found to reproduce the CLV of the data reasonably well. It is confirmed that the fluxtube temperature structure is a function of the filling factor. Amplitudes of non-stationary velocities in fluxtubes are determined from an analysis of line widths. It is found that the rms velocity amplitude does not decrease when approaching the limb, in contrast to what would be expected if the mass motions were mainly vertical. Instead, the total rms velocity is actually found to increase somewhat. Possible explanations are given, the most plausible being that the lines are broadened by a combination of wave modes having horizontal velocity components, as well as by the jiggling of fluxtubes due to the surrounding granulation.

Key words: solar magnetic fields – active regions – fluxtubes – velocity

1. Introduction

With the development of the Fourier Transform Spectrometer (FTS) of the National Solar Observatory's McMath telescope into a Stokes polarimeter at the end of the 1970s a powerful new tool for deriving fluxtube properties was introduced, allowing new diagnostic techniques to be developed and applied (see e.g. Stenflo et al., 1984). The simultaneous recording of a large number of fully resolved polarized line profiles (spanning a spectral range of typically 1000 Å) created the possibility of using the extracted line parameters as input for a statistical analysis. Thus new insight into the temperature and velocity structure of fluxtubes could be obtained (Solanki and Stenflo, 1984, 1985; Solanki, 1986).

However, these analyses have all been restricted to data obtained in a few regions near disk centre. On the other hand, the few investigations of the centre to limb variation (CLV) of Stokes parameters observed outside sunspots are without exception based on only a few lines (e.g. Howard and Stenflo, 1972; Gopasyuk et al., 1973; Stenflo et al., 1987; Solanki et al., 1987). The aim of the present paper is to combine the advantages of a many-lines analysis with the additional information contained in the CLV. We shall investigate the Stokes I and V profiles of a large number of unblended Fe I spectral lines observed in active regions at different values of $\mu = \cos\theta$ (θ is the angle between the line of sight and the vertical direction in the atmosphere). We consider various line parameters, e.g. the asymmetry and zero-crossing wavelength of Stokes V and the line depth and width of the integrated V profile. In this manner we extract further information on the velocity and temperature structure of solar magnetic fluxtubes. Due to the higher noise in our Stokes Q data than in Stokes V, a statistical analysis of this Stokes parameter is more problematic at present, and we refrain from carrying it out here. The data we shall use and the methods of obtaining them have been described by Stenflo et al. (1984, 1987). We therefore restrict ourselves to a brief summary, and refer to these papers for further information. We investigate in greater detail nine of the ten regions studied by Stenflo et al. (1987). The region observed nearest the limb ($\mu = 0.1$) has not been included, since the noise, probably induced by seeing (the limb is only 5″ away), is very large. This region also appears atypical in some of its other properties (e.g. the large inclination of the field found by Solanki et al., 1987, or the presence of a downflow seen by Stenflo et al., 1987). A summary of the data employed in the present paper is given in Table 1. Note that the two spectra nearest disk centre ($\mu = 0.98$ and 0.92) have different wavelength ranges from the rest.

2. Data reduction and method of analysis

First the data are reduced (i.e. the spectral profile of the predispersor is compensated for, etc.) as described by Stenflo et al. (1984, 1987). Next the S/N ratio of Stokes V is increased by Fourier smoothing, as described in Sect. 2.2. In order to obtain a

Send offprint requests to: S.K. Solanki

Table 1. Summary of observational data

Number	μ	Date	Type of region	Wavelength range	Spectral resolution	Integration time	Spatial resolution	Limb direction	Stokes parameters
1	0.16	84.5.3	Plage	4883–6002	523'000	43′	5″	W	*IVQ*
2	0.28	84.5.3	Plage	4883–6002	523'000	43′	5″	W	*IVQ*
3	0.30	84.5.4	Plage	4883–6002	523'000	58′	5″	W	*IVQ*
4	0.45	84.5.4	Plage	4883–6002	523'000	43′	5″	W	*IVQ*
5	0.57	84.5.4	Plage	4883–6002	523'000	65′	5″	W	*IVQ*
6	0.67	84.5.4	Plage	4883–6002	523'000	43′	5″	W	*IVQ*
7	0.83	84.5.4	Network	4883–6002	523'000	58′	5″	W	*IVQ*
8	0.92	79.4.30	Plage	4524–5580	420'000	35′	10″	SW	*IV*
9	0.98	79.4.29	Network	4566–5580	420'000	52′	10″	SE	*IV*

maximum of information on fluxtube physics we then employ the technique applied successfully to FTS data at disk centre, i.e., we carry out a statistical analysis involving multivariate regressions of line parameters determined from the recorded spectra: The line parameters are presented in Sect. 2.1, the regression equations in Sect. 2.3.

2.1. *Line parameters*

In the following we briefly describe the parameters used here. A more detailed description can be found in Solanki (1987b). Our analysis is to a large extent based on a comparison of Stokes I with I_V. Due to the generally small filling factors and the limited spatial resolution the observed Stokes I is formed mainly outside the magnetic elements. I_V is the symbol for the integrated V profile, which is a good approximation of the (not directly observable) unsplit Stokes I profile in the fluxtubes (cf. Solanki and Stenflo (1984, 1985) for a detailed description and discussion). Both profiles are parameterised identically. We represent the line depth normalised to the continuum intensity by d_I for Stokes I and d_V for I_V, respectively. Recall that for the I_V profile the line depth is fixed only up to a factor proportional to the net line of sight magnetic flux in the resolution element. However, this is the same for all lines and need not concern us further, since we only consider the lines relative to each other. We shall follow the approach used earlier and normalise d_V through comparison with model calculations (e.g. Solanki and Stenflo, 1984). The width at half minimum is represented by v_{D_I}, respectively v_{D_V}. It is given in velocity units and is expressed via the Doppler width of a gaussian having the same half width. The line strength is represented by the area of the lower half of the line. It is symbolised by S_I, respectively S_V, and is expressed in Fraunhofer (F). Besides these parameters of Stokes I and I_V we also make use of the absolute amplitudes (a_b, a_r) and absolute areas (A_b, A_r) of the blue and red wings of Stokes V, as well as of its zero-crossing wavelength, λ_V.

We have tested how well the unsplit I_V profile reproduces the Stokes I profile by comparing synthetic I_V and unsplit I profiles calculated in the same atmosphere. We find that for $g \leq 2$ the I_V profile is an excellent approximation, and it is still useful even for lines with $g=3$. The sample of unblended Fe I lines we use was originally selected by Stenflo and Lindegren (1977).

2.2. *Fourier smoothing*

For reasons discussed by Stenflo et al. (1987) the data obtained in 1984 (at various μ) have a significantly lower signal to noise (S/N) ratio than those obtained in 1979 (only near disk centre) and consequently have to be smoothed. There are many ways of smoothing a noisy profile, but probably the most common in astrophysics consists of a simple convolution with an appropriate sinc-function (for more details see Brault and White, 1971). From the Fourier convolution theorem it follows that this procedure is equivalent to a multiplication in the Fourier transform domain with the transformed distribution, which in the case of a sinc-function is a simple rectangular function. This process is equivalent to a reduction of the spectral resolution, the sinc-function being similar to the FTS apparatus function.

The choice of the number of points to be set to zero reduces to a compromise between the conservation of the profile shapes and the suppression of the noise. We have been careful to compare both smoothed and unsmoothed individual profiles and scatter plots of line parameters with each other. The spectral resolution of our data being extremely high, it has been possible to cut off a relatively large number of discrete Fourier frequencies, thus suppressing much of the disturbing noise, while keeping the profiles practically free from distortions. However, even after this procedure the scatter (in the data of 1984) is still considerably larger than for the data at disk centre (from 1979). As in the previous papers we have also discarded the lines whose signal is small as compared with the noise level. However, in order to retain a significant sample of lines we have been somewhat less restrictive in our choice of useful lines (S/N > 4).

2.3. *Regression analysis*

Each line parameter of I_V, Stokes I, or Stokes V is a function of a number of other line attributes (e.g., line strength S_I, excitation potential χ_e, effective Landé factor g_{eff}, wavelength λ), of intrinsic properties of the observed solar region (e.g., magnetic filling factor α, fluxtube temperature T, mass motions, magnetic field strength B), and of observational parameters (e.g., cosine of the heliocentric angle μ, S/N ratio, spectral resolution). Furthermore, the various variables are interconnected, e.g., the line strength depends on the transition probability, abundance, temperature, and to a lesser extent also on mass motions and the magnetic field strength. The final aim of our analysis is to derive the intrinsic properties of fluxtubes. Therefore, we must first separate the various dependences of a line parameter from each other as well as possible, and then interpret each in terms of fluxtube properties.

A multivariate regression analysis appears to be the appropriate technique for tackling the first part of this problem, while

model calculations are often required to make progress in the second part. This is exactly the approach adopted in the previous papers of this series, which, however, only considered data near disk centre. The previously considered spectra were all obtained at practically the same μ value, they have very high spectral resolution and good S/N ratios. In the present paper we extend the analysis to data obtained at various positions on the solar disk. Due to the considerably lower S/N ratio, the noise-induced scatter in the line parameters is greatly increased, overshadowing the usually small dependences on χ_e, g_{eff}, and λ. This is often the case even after the smoothing procedure described in Sect. 2.2. Furthermore, since we are now comparing regions with quite different α and μ values with each other, we will also have to include these two parameters in the regressions. In order to take both these factors into account adequately, while at the same time avoiding cumbersome regression equations, we have carried out the regressions in a slightly different manner than in the previous papers, namely in two steps. First we make a regression of the given line parameter according to line strength only. We carry out least squares fits to the data points with a polynomial, its degree being determined by the well known statistical F-test (which can be used to test the significance of adding a higher order term to a given polynomial). We find that all the scatter plots we investigate here can be fitted adequately by second order polynomials in line strength of the form

$$y = a_0 + a_1 S_I + a_2 S_I^2. \quad (1)$$

Here y represents the values of any line parameter or combination of line parameters, such as v_{D_V} or $\ln(d_V/d_I)$, and the a_i are the regression coefficients. A regression of the type of Eq. (1) is carried out for each of the nine observed regions, so that we finally have 9 values for each regression coefficient. In a second step we make a regression of the regression coefficients obtained in the first step, a_i, according to μ and α using an equation of the form

$$a_i = b_{0,i} + b_{1,i}\alpha\mu + b_{2,i}\alpha. \quad (2)$$

We have also tried to fit the data using other combinations of α, μ, and $\alpha\mu$, but these trials were statistically less successful for almost all line parameters (an exception is discussed in Sect. 3.3). We are well aware that a regression involving three coefficients of only nine data points is at the limit of what is reasonable, and stress that the above equation is not meant to be exhaustive, but is of an exploratory nature. It is thought of as being a qualitative description of a (probably) more complex relationship connecting the appropriate line parameter with the filling factor and μ. The α values for the various observed regions have been taken from Solanki et al. (1987), these being the best existing estimates. However, they must be treated with some caution (like all other determinations of α to date), since it has been recently argued that all empirically determined α values are rather unreliable due to the unknown continuum contrast of fluxtubes (Grossmann-Doerth et al., 1987; Schüssler and Solanki, 1987).

3. Data analysis

3.1. The relative amplitude asymmetry

Ever since its discovery (Illing et al., 1974; Stenflo et al., 1984) the physical source of the Stokes V asymmetry has remained unclear. Basically two models have been proposed for its production, namely velocity gradients (Illing et al., 1975) and atomic orientation (Kemp et al., 1984). At present neither mechanism can be ruled out, although it can be shown that velocity gradients of *stationary* flows cannot account for the observations. Both further observations and model calculations are required to settle the question of the source of the asymmetry. In this context an empirical many-lines centre-to-limb analysis of the asymmetry is of interest, in particular since Stenflo et al. (1987) have observed the area asymmetry of a few medium strong lines to change sign near the limb. In this section we consider the CLV of the amplitude asymmetry, while the area asymmetry is discussed in the next section.

The relative amplitude asymmetry is defined as $\delta a = (a_b - a_r)/(a_b + a_r)$. We are interested in the asymmetry as a function of essentially three parameters, the line strength, μ, and the filling factor. For maximum clarity we have chosen to use more than one representation of the data. First in Fig. 1 we show δa as a function of S_I at two positions on the solar disk ($\mu = 0.67$ in Fig. 1a and $\mu = 0.28$ in Fig. 1b). Stars represent Fe I lines with $\chi_e < 3$ eV, while circles represent Fe I lines with $\chi_e \geq 3$ eV. Note the scarcity of weak lines with $\chi_e < 3$ eV. These lines are so greatly weakened inside fluxtubes that they are usually strongly affected by noise. The two solid curves bound the data points lying within one standard deviation of the mean. They were calculated by averaging the points within intervals of width $\Delta S_I = 1.5$ F. This figure clearly

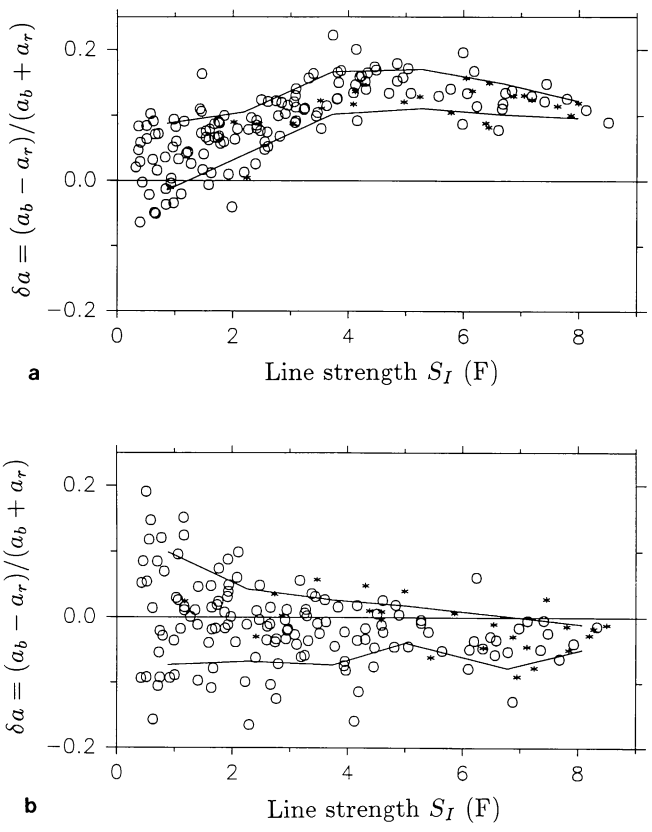

Fig. 1a and b. Relative amplitude asymmetry of Stokes V, $\delta a = (a_b - a_r)/(a_b + a_r)$, vs. Stokes I line strength, S_I. a_b and a_r are the absolute blue and red amplitudes of Stokes V, respectively, **a** Data obtained in an active region plage at $\mu = 0.67$. The two curves bound the points within 1σ of the mean. Stars represent low excitation Fe I lines with $\chi_e < 3$ eV, the circles mark lines with $\chi_e \geq 3$ eV. **b** Data obtained in an active region plage at $\mu = 0.28$

shows that the difference in the Stokes V asymmetry of the two regions is significantly larger than the scatter in the data.

Since only two lines with $S_I > 9$ F are present in the data obtained in 1984 and their parameters are less reliable than in the old data due to noise, we have restricted ourselves to the range $0 \leq S_I \leq 9$ F, where a large number of points are more or less homogeneously distributed, and a statistical approach is completely justified. Note that the drop in the density of data points below 0.5 F is an effect of the selection of only those lines which lie above a certain S/N threshold.

Figure 2 shows the quadratic regression curves for all 9 selected regions plotted vs. S_I. The curves are numbered according to increasing μ as indicated in Table 1. The asymmetry evidently decreases when approaching the limb, in particular for lines having strengths greater than 3 F. δa actually appears to become slightly negative for these lines at $\mu \leq 0.30$. For weaker lines one hardly recognizes any dependence on limb position. This becomes more evident in Fig. 3a, where we have plotted the coefficient of the constant term, a_0, vs. μ (cf. Eq. (1)). The straight line is a least squares fit to the $a_0(\delta a)$ points. The values seem to be distributed rather stochastically around zero. This interpretation is supported by the fact that the α, μ regression of a_0 does not show any significant dependence on either parameter. Reasons for the considerable scatter in Fig. 3a are the relatively small number of very weak lines in our sample and the great uncertainty, due to the small signal to noise ratio, in the determination of their asymmetries. In Fig. 3b the coefficient a_1 has been plotted vs. μ. It is interesting to note (but not easy to interpret) that the CLV of $a_1(\delta a)$ is rather similar to the CLV of δA for the medium strong lines considered by Stenflo et al. (1987). A regression of the type of Eq. (2) shows that much of the scatter around the least squares fit in Fig. 3b is due to the dependence of a_1 on α (both $b_{1,1}$ and $b_{2,1}$ are significant at the 3σ level). The dependence on α is found to increase towards the limb. A look at Fig. 3c shows that a_2, the curvature of δa as a function of S_I, is a function of μ as well, being minute for $\mu \lesssim 0.4$ and negative for $\mu \gtrsim 0.4$. This effect is clearly due to the rapid increase towards the disk center of the asymmetry for the lines of intermediate strength, as compared with the weak and the strong ones. The general μ dependence of the amplitude asymmetry is compatible with mainly vertical velocity gradients (or gradients parallel to the magnetic field), although the possible presence of a change in sign near the limb suggests that this conclusion should be treated with caution.

Summarizing the α, μ dependence obtained from Eq. (2) of all three regression equations we find that the total asymmetry decreases both with increasing α and decreasing μ for all but the weakest lines. This dependence on α is in accordance with the results of Stenflo and Harvey (1985).

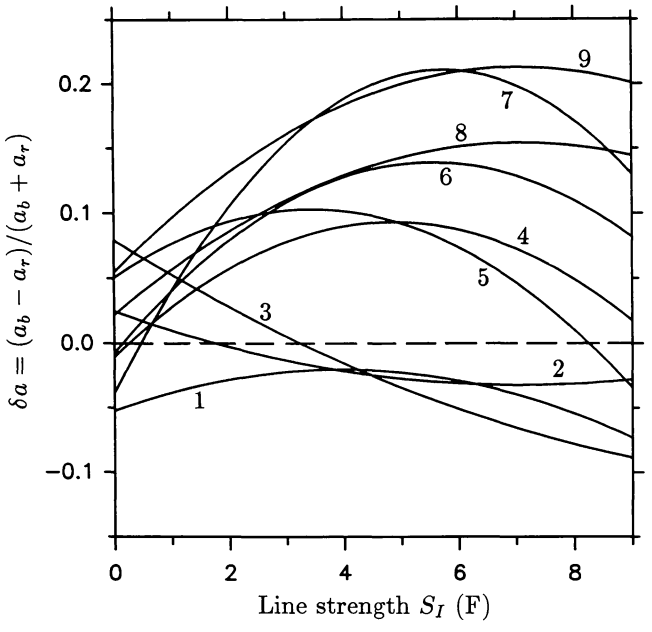

Fig. 2. Second order polynomial fits to δa vs. S_I for all nine regions studied. The zero line is plotted dashed. The curves are numbered as in Table 1

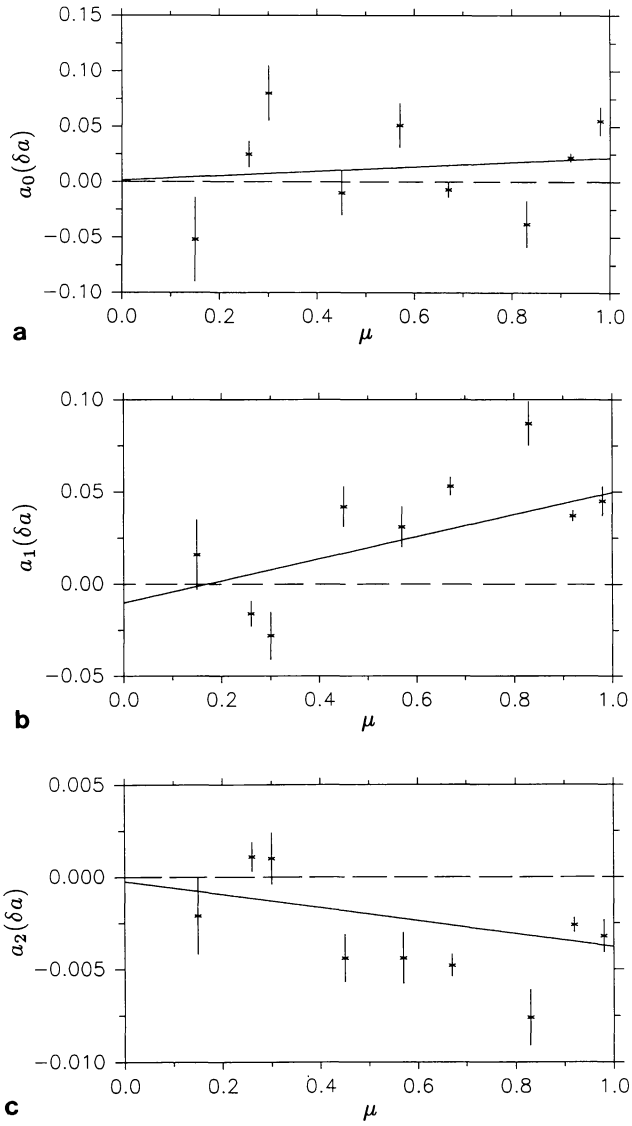

Fig. 3a–c. The coefficients of the second order polynomial fits to δa [cf. Eq. (1)], plotted as functions of μ. The solid straight lines are least squares fits. **a** Zeroth order coefficient a_0. **b** First order coefficient a_1. **c** Second order coefficient a_2

3.2. *The relative area asymmetry*

In analogy with δa we define a relative area asymmetry $\delta A = (A_b - A_r)/(A_b + A_r)$. In Fig. 4 δA has been plotted vs. S_I for the same two regions as in Fig. 1. The strongly negative δA for the lines with $S_I \gtrsim 3$ F in the region at $\mu = 0.28$ clearly confirms the change in sign observed by Stenflo et al. (1987), which was based on only a few spectral lines near $\lambda = 5250$ Å. Figure 5 is the area asymmetry counterpart of Fig. 2. A surprising feature of Fig. 5, when compared with Fig. 2, is the less clear evidence of a μ-dependence. The amplitude being more sensitive to noise one would expect exactly the opposite effect. Nevertheless, we see a tendency for the area asymmetry to become increasingly negative with decreasing μ. The dependence on μ appears to be largest for the strong lines. Near disk centre only the strongest lines have a slightly negative δA, but as we go towards the limb, weaker and weaker lines obtain a negative δA. Thus at intermediate μ values significant numbers of lines with both signs of the asymmetry are present in one and the same spectrum. At least for the observed regions the change in δA with μ appears to be more gradual than in δa. A comparison of Fig. 5 with Fig. 2 shows that considerable differences exist between δA and δa. For example, the lines with $S_I \gtrsim 5$ F in the two regions around $\mu = 0.5$ (Nos. 4 and 5) exhibit negative δA, while their δa is still positive. Note that the maximum absolute value of δA is larger for regions near the limb than near disk centre. This may signify that horizontal v and B gradients are larger than the vertical ones (if δA is a result of velocity gradients).

While the coefficients of the linear and the quadratic terms (plotted vs. μ in Figs. 6b and c) show trends similar to those exhibited by $a_1(\delta a)$ and $a_2(\delta a)$ in Figs. 3b and c, we find that $a_0(\delta A)$ of all the regions is consistent with a positive area asymmetry for the weakest lines (Fig. 6a). This result could have important consequences for identifying the mechanism underlying the area asymmetry of Stokes V. Velocity gradients of all types, produced either by stationary or non-stationary flows are expected to produce a negligible area asymmetry in very weak lines with practically no saturation (Solanki, 1987b). If the positive values of $a_0(\delta A)$ are significant, then velocity gradients cannot be alone responsible for the observed δA. However, Fig. 6a can only be considered a (weak) indication in this direction. Observations with higher S/N ratios of a few weak lines are required to provide a more reliable answer.

The α dependence of δA is less clear than of the amplitude asymmetry, being at the 2σ level in the regression Eq. (2). δA shows a tendency to decrease with increasing α.

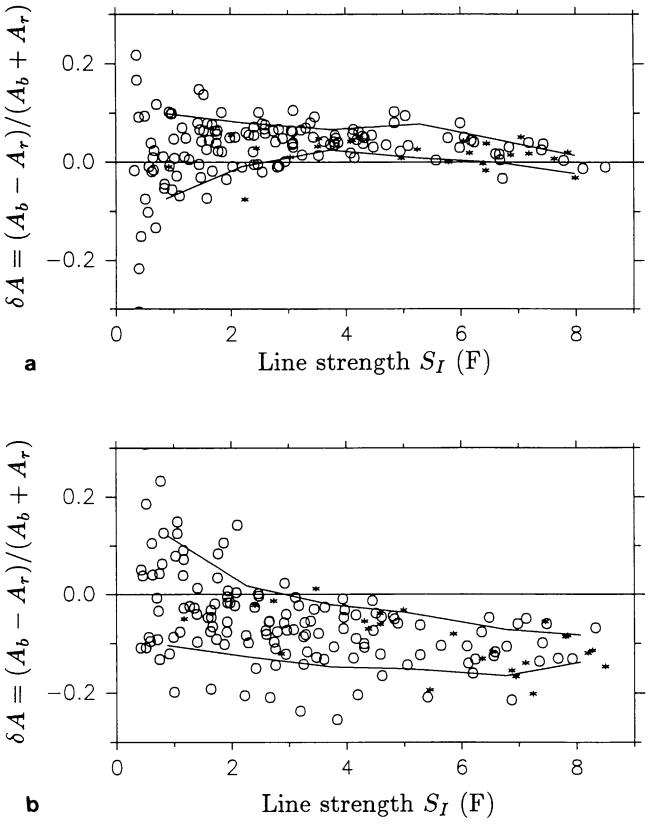

Fig. 4a and b. Relative Stokes V area asymmetry $\delta A = (A_b - A_r)/(A_b + A_r)$ vs. S_I. A_b and A_r are the absolute areas of the blue and red wings of Stokes V, respectively. **a** $\mu = 0.67$ (upper figure). **b** $\mu = 0.28$ (lower figure)

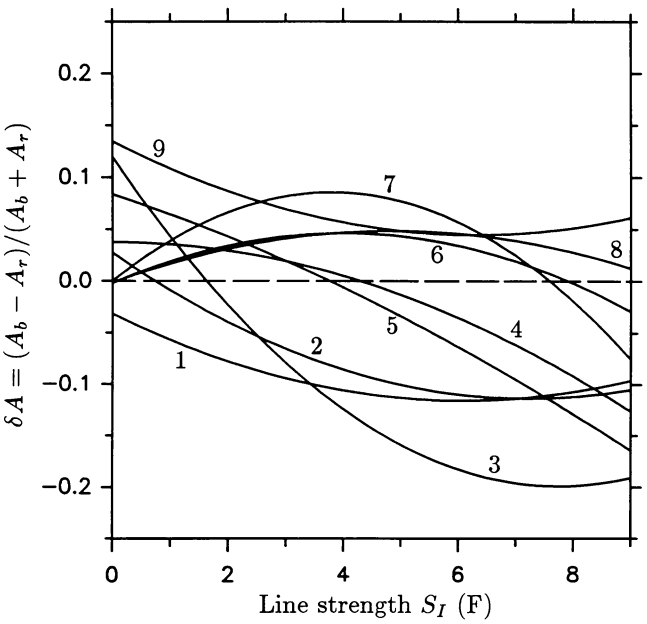

Fig. 5. Second order polynomial fits to δA vs. S_I for all nine investigated regions. The zero line is plotted dashed. The curves are numbered as in Table 1

3.3. $\ln(d_V/d_I)$ *and fluxtube temperature*

Solanki and Stenflo (1984) discovered that the shape of the $\ln(d_V/d_I)$ vs. S_I scatter plot is very sensitive to fluxtube temperature, while the absolute value of $\ln(d_V/d_I)$ is also a function of filling factor. In this section we discuss some of the results which can be extracted directly from this scatter plot without recourse to model calculations. The results of model calculations will be discussed separately in Sect. 4.2. In Fig. 7a the constant terms a_0 (stars) of the quadratic regressions of the type of Eq. (1) for $\ln(d_V/d_I)$ are plotted vs. the filling factor α determined by Solanki et al. (1987).

The tightness of this correlation may be fortuitous, since we expect a_0 to be a function not only of α, but also of δ_c, $\cos\gamma$, T, and μ, where $\delta_c = I_c^{\text{Fluxtube}}/I_c^{\text{Photosphere}}$ is the continuum contrast, γ is the angle between the line of sight and the magnetic field, and T is the fluxtube temperature, which is itself a function of α. A chance

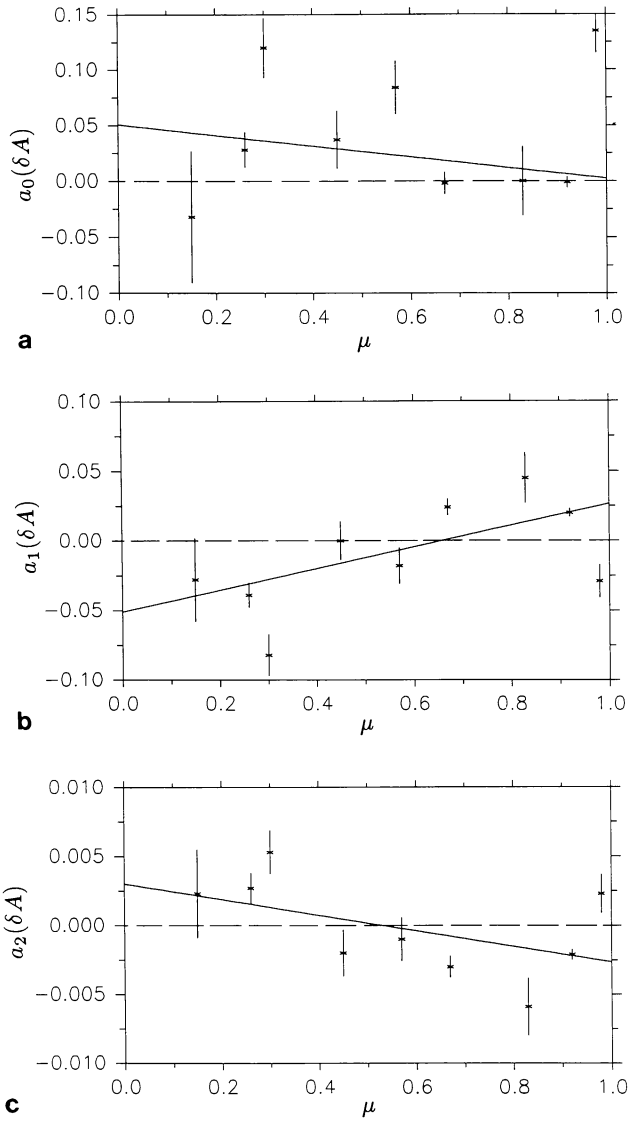

Fig. 6. Same as Fig. 3 for the coefficients of the second order polynomial fits to δA

correlation between the other variables may, for our limited set of observations, induce an enhanced correlation between a_0 and α.

We have tested the dependence of a_0 on a further parameter, namely μ, with biregressions of various forms, the most successful of which is:

$$a_0 = b_0 + \mu b_1 + \alpha\mu b_2 .$$

It shows that a_0 is also dependent on μ as well as on α.

As pointed out by Solanki and Stenflo (1984) the information about the temperature structure of fluxtubes is mainly contained in the gradient of the $\ln(d_V/d_I)$ plot. The depth of formation of the weak lines being much more sensitive to temperature than that of the strong ones, it follows that a temperature increase inside the fluxtubes makes the curves in this plot steeper. $a_1(\ln(d_V/d_I))$ should therefore be the most temperature sensitive of the three regression coefficients. Figure 7b shows its dependence on α. The circles are data points, while the curve is a second order least squares fit to them; the straight lines are discussed later. As expected from previous investigations, a_1 decreases initially with increasing filling factor. However, for $\alpha \gtrsim 20\%$ a_1 begins to increase once more. This seems to contradict the observational fact that very high filling factor features like sunspots and pores are cooler than plage and network fluxtubes. An explanation of the strange behaviour of a_1 can be given if one assumes that a_1 depends on μ as well. The straight lines have been calculated by setting $\mu = 0.0, 0.2, \ldots, 1.0$, respectively ($\mu = 0.0$ corresponds to the steepest line) after applying regression Eq. (2), i.e., the straight lines show what the α dependence would be for data at a given fixed μ.

The fact that a_1 becomes negative close to the limb for large α is probably an artifact of the linear form of the regression equation. Higher order regressions on the other hand need too many free parameters for our nine data points. We have mainly shown here that the dependences on μ and α are of approximately the same magnitude. Furthermore, we expect the $\ln(d_V/d_I)$ vs. S_I curves to become less steep for increasing α as well as for a decreasing μ. This dependence on α is consistent with a decrease in fluxtube temperature for regions with larger magnetic flux (cf. Solanki and Stenflo, 1984). The dependence on μ cannot be discussed without recourse to model calculations. These relations imply that the lines in fluxtubes are more strongly weakened (relative to the local quiet sun) near disk centre than near the limb, and in regions with small filling factors than in regions with large ones. In Fig. 7c a_2 is plotted vs. α, both for the data (which have again been fitted by a parabola) and for the results of regression Eq. (2) reduced to different values of μ (straight lines; once more the steepest line corresponds to $\mu = 0$). As expected a_2 shows a dependence on α opposite to that of a_1.

Since the Stokes I profiles in active regions are also affected somewhat by the presence of fluxtubes it would be better to use d_I from spectra obtained in the quiet sun. Otherwise it is difficult to decide how much of the α dependence of $\ln(d_V/d_I)$ is really due to changes in fluxtube temperature. Unfortunately, such spectra are unavailable at the appropriate μ values for most of the regions, so that d_I had to be taken from the same active region as d_V. However, for the regions with $\mu = 0.30$ and 0.28 we have also used an FTS spectrum (containing Stokes I only) obtained in a quiet region at a similar μ by P.N. Brandt. We find that through the use of quiet sun d_I values the $\ln(d_V/d_I)$ vs. S_I curves are not significantly changed, and these two regions alter their positions in Figs. 7b and c only slightly. Since according to Solanki et al. (1987) the active region at $\mu = 0.28$ has one of the larger filling factors of our sample, we conclude that the use of the active region Stokes I profiles does not significantly degrade our analysis, and the conclusions drawn from Figs. 7b and c should remain valid. We wish to note, however, that $v_{D_V} - v_{D_I}$ is changed in a manner which implies that active region Stokes I profiles are broader than the corresponding quiet sun profiles.

3.4. Stokes V zero-crossing wavelength shifts

We have analysed the shift of the Stokes V zero-crossing wavelength with respect to both Stokes I and laboratory wavelengths. Details of the exact procedure for determining Stokes I and V wavelengths etc. may be found in Solanki (1986). The only difference in methodology with respect to that paper is that when determining absolute wavelengths for the solar data the Mg I b 5172.7 Å line has always been used as a reference to eliminate

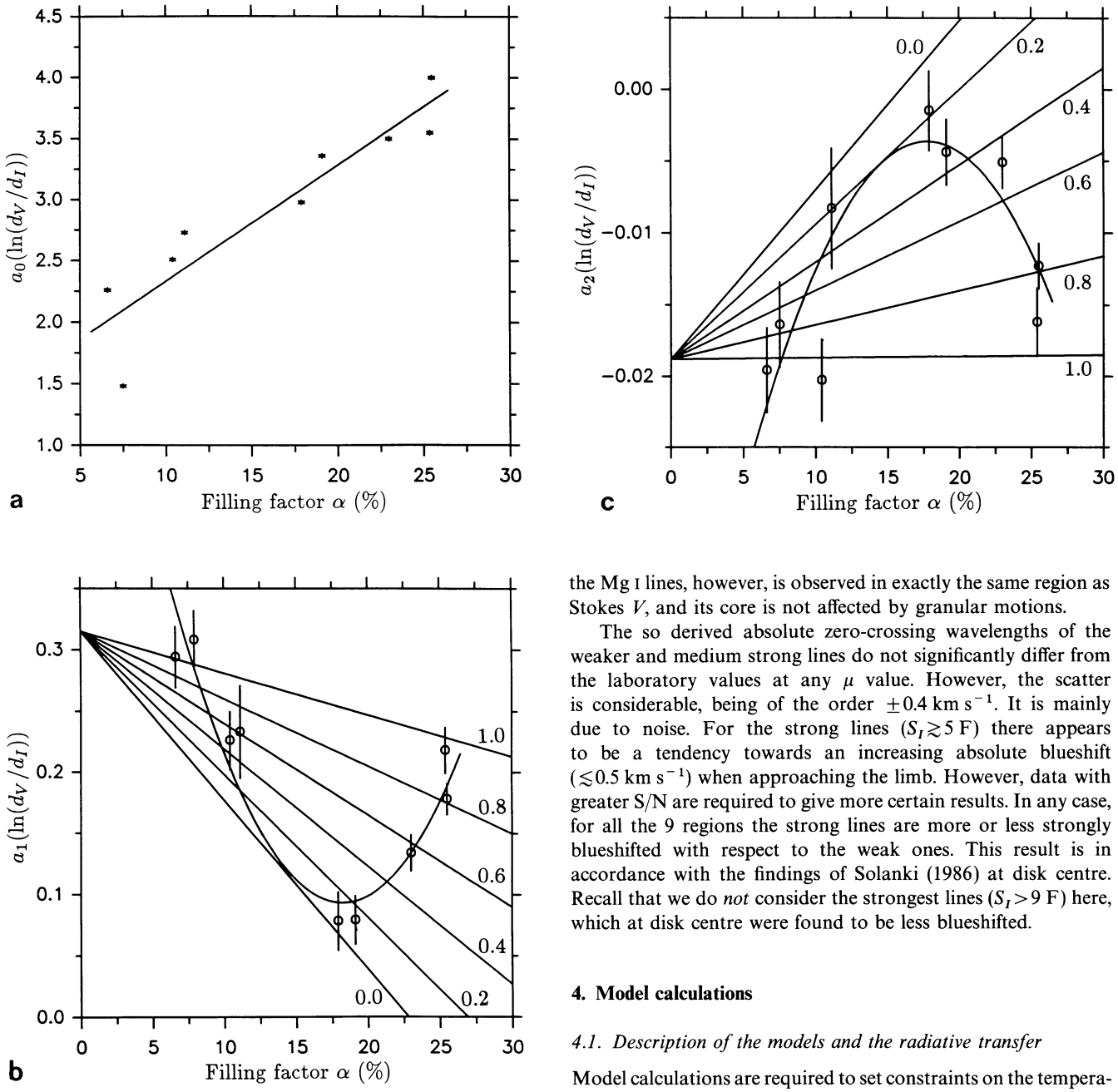

Fig. 7a–c. The coefficients of the second order polynomial fits to $\ln(d_V/d_I)$, plotted as a function of filling factor. **a** Coefficient of the constant term, a_0. The straight line is a least squares fit. **b** Coefficient of the linear term, a_1. The parabola is a least squares fit to the data points. The straight lines illustrate the dependence of a_1 on α once its dependence on μ has been compensated for using Eq. (2). The uppermost line corresponds to the α dependence of $a_1(\ln(d_V/d_I))$ at $\mu=1$, the others to $\mu=0.8, 0.6, 0.4, 0.2, 0.0$, respectively, as marked in the figure. **c** Same as **b** for the coefficient of the second order term, a_2. $\mu=1$ corresponds to the lowest straight line in this figure

solar-terrestrial relative motion, solar rotation, and gravitational redshift. We have adopted this approach, originally proposed by Livingston (1983), since near the limb even a small uncertainty in the position of the FTS entrance aperture can have a large influence on the deduced velocity of solar rotation. The I profile of the Mg I lines, however, is observed in exactly the same region as Stokes V, and its core is not affected by granular motions.

The so derived absolute zero-crossing wavelengths of the weaker and medium strong lines do not significantly differ from the laboratory values at any μ value. However, the scatter is considerable, being of the order ± 0.4 km s^{-1}. It is mainly due to noise. For the strong lines ($S_I \gtrsim 5$ F) there appears to be a tendency towards an increasing absolute blueshift ($\lesssim 0.5$ km s^{-1}) when approaching the limb. However, data with greater S/N are required to give more certain results. In any case, for all the 9 regions the strong lines are more or less strongly blueshifted with respect to the weak ones. This result is in accordance with the findings of Solanki (1986) at disk centre. Recall that we do *not* consider the strongest lines ($S_I > 9$ F) here, which at disk centre were found to be less blueshifted.

4. Model calculations

4.1. Description of the models and the radiative transfer

Model calculations are required to set constraints on the temperature structure inside fluxtubes as well as to quantitatively determine the amplitudes of the velocities giving rise to the large observed Stokes V line widths. We have decided to restrict our calculations to the plage and the network models described by Solanki (1986), since these models have previously been able to reproduce extensive data near disk centre, as well as the CLV of the Stokes Q asymmetry (Solanki et al., 1987). The magnetic field is calculated in the thin fluxtube approximation, i.e. as the square root of the pressure difference between the fluxtube interior and the surrounding non-magnetic atmosphere. The field strength has been chosen such that the results are consistent with line ratio measurements [i.e. $B(\tau=1)=2000$ G]. However, since we have generally calculated only lines with very small $g_{\rm eff}$ values for comparison with the scatter plots, the actual strength of the field is unimportant for most of the following analysis. The external atmosphere is represented by the HSRASP (Chapman, 1979;

Gingerich et al., 1971; Spruit, 1974). Only one line of sight, having an angle θ with the fluxtube axis is considered (θ is the heliocentric angle). This means that we have assumed the fluxtubes to be well approximated by a plane parallel atmosphere with the magnetic field being vertical to the solar surface. Due to the small horizontal extent of the magnetic structures the assumption of a plane parallel atmosphere is even less applicable near the limb than at disk centre. However, we want to obtain an overview of the information in the rather extensive data set, and a complete 1.5-D calculation using cylindrical fluxtubes would be extravagant. The assumption of a vertical field does not adversely affect the determination of velocity or temperature from Stokes V, in particular since the Zeeman splitting of most of the used lines is small. The code used for the radiative transfer consists of a modified version of the one described by Beckers (1969a, b), which assumes LTE and enables the general computation of Zeeman-split line profiles. More details regarding the models and the radiative transfer are to be found in Solanki (1986, 1987b).

We have calculated $\ln(d_V/d_I)$ for a set of 7 hypothetical lines having various line strengths in the range $0.5\ \mathrm{F} \lesssim S_I \lesssim 8\ \mathrm{F}$, using both the network and the plage models of Solanki (1986). The use of hypothetical lines is quite appropriate for LTE calculations, since it saves computer time. All lines have $g_{\mathrm{eff}}=0$, $\chi_e=3$ eV, and $\lambda=5500$ Å. We have not calculated lines with different χ_e, g_{eff}, and λ for the same reasons as why we did not carry out any regressions with these parameters (Sect. 2.2). In addition to these hypothetical lines we have also used the ten lines listed in Table 1 of Solanki (1986), plus the Fe I lines at 5127.36 Å (multiplet 16, $\chi_e=0.91$ eV, $S_I=6.66$ F, $g_{\mathrm{eff}}=1.5$). The calculated Stokes I profiles of these lines are compared with their complete observed I_V profiles individually.

We use the classical formula of Unsöld (1955) to calculate the Van der Waal's damping constant, $\Gamma_{\mathrm{Unsöld}}$. Following Holweger (1979) and Simmons and Blackwell (1982) we also introduce an empirical correction factor δ_Γ, defined by $\Gamma_{\mathrm{true}}=\delta_\Gamma\Gamma_{\mathrm{Unsöld}}$. For Fe I lines with $\chi_e \leq 4$ eV we either directly use the δ_Γ values listed by Simmons and Blackwell (1982) as a function of multiplet number or extrapolate from those. For Fe I lines with $\chi_e > 4$ eV and for Fe II lines we set $\delta_\Gamma=2.5$ in accordance with Holweger (1979).

4.2. Calculations of the CLV of $\ln(d_V/d_I)$ and the temperature in fluxtubes

Comparison of calculated $\ln(d_V/d_I)$ vs. S_I curves with the observed scatter plots can lead to conclusions about the temperature structure of the fluxtubes in the observed region.

In order to separate the influence of temperature and velocity on the CLV of the $\ln(d_V/d_I)$ vs. S_I plot, we have calculated our set of hypothetical lines in the quiet sun atmosphere, in the two fluxtube models and in a model with $T(\tau)$ approximately 400 K hotter than the $T(\tau)$ of the HSRA everywhere. Different amounts of velocity broadening have been tried, namely no velocity broadening at all, only a microturbulence broadening, and various mixtures of micro- and macroturbulence. Finally, we have also attempted to fit the line depths and widths by varying the turbulence velocity. More details are given in Sect. 4.3.

If we determine d_V using the model with $T(\tau)$ parallel to the temperature structure of the HSRA, while assuming no micro- and no macroturbulence in fluxtubes and the quiet sun, then $\ln(d_V/d_I)$ vs. S_I shows only a very weak CLV. Although the lines in the fluxtubes do get somewhat strengthened as compared with the quiet sun profiles near the limb, it is much less than the strengthening observed in the data after accounting for variations due to the filling factor (Sect. 3.3). The CLV of $\ln(d_V/d_I)$ changes dramatically, as soon as we broaden the lines in the external atmosphere with a mixture of micro- and macroturbulence, but leave the fluxtube line profiles unbroadened. It then looks much more similar to the observations. However, the calculated line widths of the profiles inside the fluxtubes are much too small. They require broadening by a mixture of macro- and microturbulence as well (Sect. 4.3). This once more reduces the CLV and destroys the fit to the observed $\ln(d_V/d_I)$.

The case is quite different for the plage model. Figure 8a shows $\ln(d_V/d_I)$ vs. S_I as calculated with the plage fluxtube model for eigh different values of μ ranging from 0.15 to 0.98. The curve for $\mu=0.92$ has not been plotted since it lies very close to that of the region at $\mu=0.98$. In this figure all the line profiles are unbroadened by any velocity. It is clear from the figure that the relative line weakening inside the fluxtube decreases appreciably as we approach the limb. This is also the case for the network model. Qualitatively the same picture also results when the lines are broadened by microturbulence, or for example when using similar amounts of micro- and macroturbulence in quiet sun and fluxtube. When comparing with the CLV of $\ln(d_V/d_I)$ of the model with temperature structure parallel to that of the HSRA, the main difference is due to the steeper gradient of $T(\tau)$ in the plage model at the level at which the weak lines are formed ($-2.0 \lesssim \log\tau \lesssim -1.0$). As a result of the increasing heights of formation close to the limb, the weak lines in the plage model are formed at lower temperatures near the limb and are consequently more strengthened in comparison with the model with $T(\tau)$ parallel to the HSRA. In Fig. 8b we have plotted $\ln(d_V/d_I)$ vs. S_I for the synthetic profiles at various μ after they have been broadened by velocities so that they reproduce the observed line widths (cf. Sect. 4.3). A comparison with Fig. 7b shows that Fig. 8b is (at least qualitatively) consistent with the observed behaviour of the spectral lines. The comparison between calculations and observations becomes clearer if we make least squares fits with second order polynomials to the calculated curves as well, and only compare these fits. As expected, we find a decrease in $a_1(\ln(d_V/d_I))$ with decreasing μ for the calculated lines. Quantitatively there are still some differences, which partly stem from noise in the data, but partly also from the fact that we are attempting to describe with a single temperature structure fluxtubes in different regions, which do not have the same $T(\tau)$.

These results suggest that the fluxtube has a steeper temperature gradient than the surrounding photosphere over a part of its height range. However, such an interpretation must be treated with care, since another fluxtube parameter also plays a role: the finite width of the fluxtubes, which increasingly manifests itself in the spectra closer to the limb. Its neglect leads to an increasing underestimate of the fluxtube temperature near the limb.

Figure 9 shows $\ln(d_V/d_I)$ for an active region plage observed at $\mu=0.28$ and for both the plage and the network temperature models, each with the lines broadened such that they reproduce the observed line widths. The Stokes I data have been taken from a quiet sun spectrum with a similar μ. Within the scatter, the data appear to be consistent with a fluxtube temperature lying somewhere between that of the two models. When broadened to reproduce the line widths, the models of Solanki (1986) seem to cover the range of fluxtube temperatures in our (limited) sample of

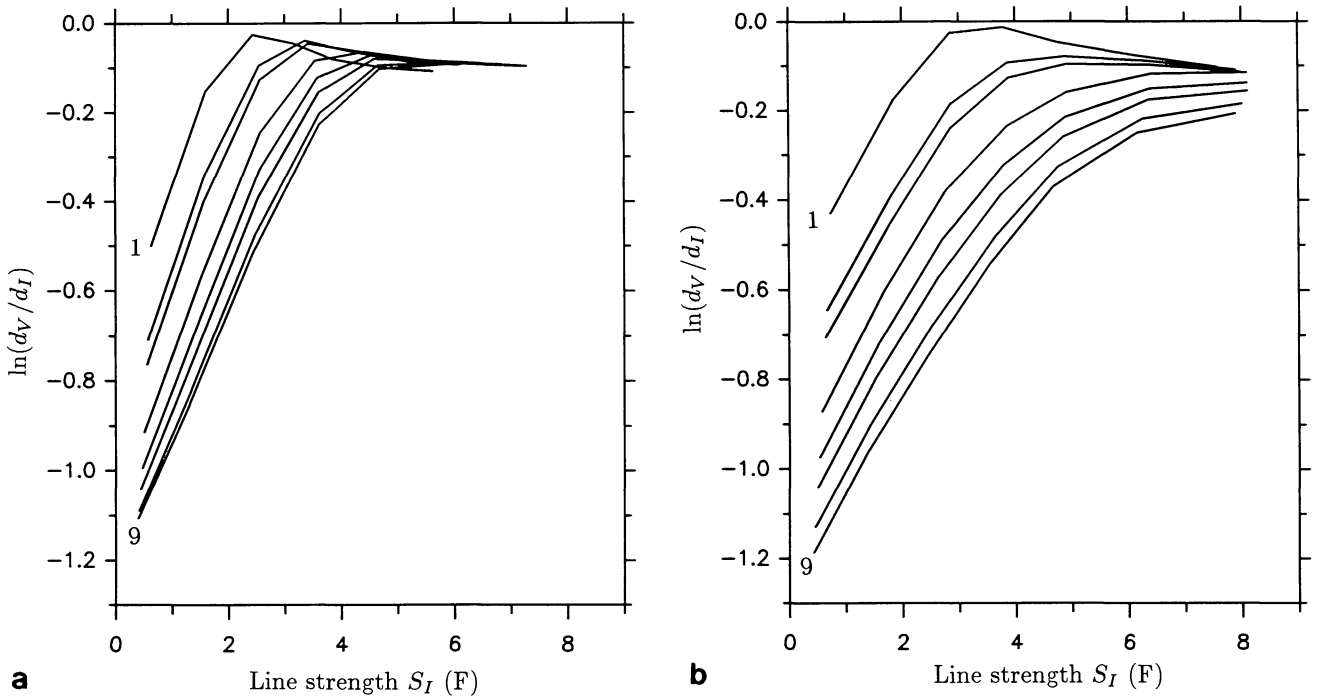

Fig. 8a and b. $\ln(d_V/d_I)$ vs. S_I as calculated with the plage model for 8 of the 9 μ values of Table 1 for which we have data ($\mu=0.92$ has not been plotted). **a** $\xi_{\rm mic}^{\rm fluxtube}=\xi_{\rm mic}^{\rm quiet}=\xi_{\rm mac}^{I}=\xi_{\rm mac}^{V}=0$ (no velocity broadening at all). **b** $\xi_{\rm mic}^{\rm fluxtube}(\mu)=\xi_{\rm mic}^{\rm quiet}(\mu)$, taken from Simmons and Blackwell (1982). $\xi_{\rm mac}^{I}$ and $\xi_{\rm mac}^{V}$ have been determined from fitting observed line widths. (For the μ values for which no quiet sun Stokes I measurements were available, the $\xi_{\rm mac}^{I}$ values have been interpolated.)

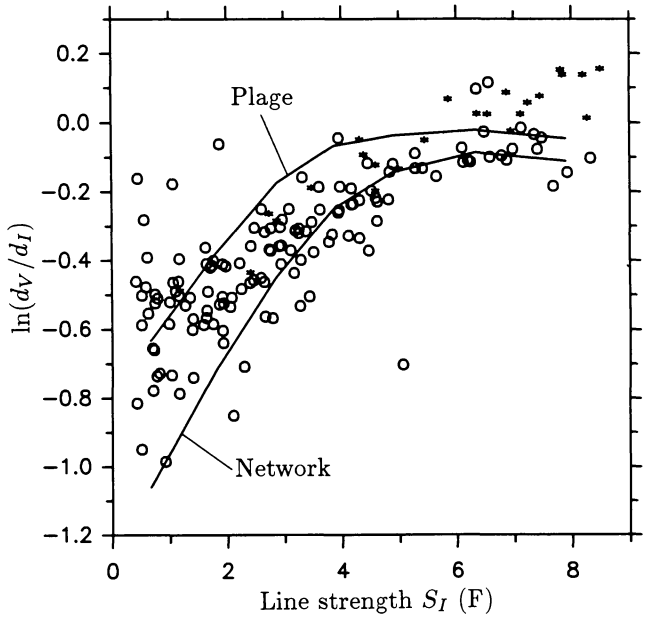

Fig. 9. $\ln(d_V/d_I)$ vs. S_I. Comparison of calculations (plage model, upper curve; network model, lower curve) with observations of an active region plage at $\mu=0.28$. Stars and circles represent low and high excitation lines, respectively (cf. Fig. 1)

observations, within the context of one dimensional models. Note, however, that the models do not provide a perfect fit. Near the limb they give $\ln(d_V/d_I)$ curves which are too humped, i.e. the medium strong lines in the fluxtubes ought to be more weakened to match the data.

4.3. Mass motions in fluxtubes from the CLV of the line widths

Although many authors have tried to measure stationary net mass-flows inside fluxtubes (see Solanki, 1987a for an overview), until recently little progress has been made concerning non-stationary velocities in them, mainly due to the fact that high quality full profile spectra in polarized light had not been previously available. As a first step Solanki (1986) showed that at disk centre the macroturbulence velocity inside fluxtubes is strongly dependent on the line strength, reaching rms values of 3–3.5 km s^{-1} for the most broadened lines. In the present section we investigate if the mass motions are restricted to a direction parallel to the field lines, or if a significant perpendicular component is present as well. We shall follow the general method outlined in Solanki (1986), describing the mass motions by a combination of micro- and macroturbulence. We stress once more that we are not thereby supposing the true mass motions inside fluxtubes to be turbulent, but rather use this approach only as an efficient way of deducing the magnitude of the line of sight velocity.

First we model the quiet sun data. We obtain $\xi_{\rm mic}(\mu)$ in the quiet sun by interpolating linearly between the μ values listed by Simmons and Blackwell (1982). The macroturbulence is determined by fitting the observed I profiles in a quiet region near disk centre and one near the solar limb observed by P.N. Brandt. The $\xi_{\rm mac}^{I}$ values at other μ are obtained by linear interpolation between these two regions (superscript^I denotes that this $\xi_{\rm mac}$ has been obtained from quiet sun Stokes I profiles). The derived $\xi_{\rm mac}^{I}$ values

are compatible with those obtained by Caccin et al. (1976) and Holweger et al. (1978). Details regarding the quiet sun ξ^I_{mac} will be given in a later paper.

Before turning to the ξ_{mac} inside the fluxtubes we wish to make a few remarks about the method. In order to determine the macroturbulence we have convoluted the computed I profiles with a Voigt function $H(a_{mac}, \xi_{mac})$ (cf. Mihalas, 1978 for a definition) so that they match the observed Stokes I or I_V profiles. We use two techniques: the first based on the analysis of the complete I_V profiles of a few selected lines, the second based on a statistical approach using the widths of the complete sample of observed Fe I lines. In order to apply the first technique, a program has been written which searches in the (a_{mac}, ξ_{mac})-plane for minima in the area enclosed between the two profiles (ideally, both profiles should have the same equivalent widths). We have also tested fitting procedures based on other quantities which must be minimised, but have found the area to be simple to implement and to exhibit stable convergence.

The choice of the wavelength window within which the lines are matched is found to be particularly important, since even a small blend in one of the line wings can affect the total fit (and thereby ξ_{mac}) considerably. We must also keep in mind that the wings of I_V are always more or less strongly disturbed by noise (since the underlying V profile is proportional to $dI/d\lambda$, which is particularly small in the far wings). The windows are much less of a problem when fitting line profiles manually, since one then easily gives a smaller weight to the blended and noisy parts of the profile.

The automated technique was first tested on both Stokes I and I_V profiles near disk centre and was found to give approximately the same values for ξ^I_{mac}, a^I_{mac}, ξ^V_{mac}, and a^V_{mac} as obtained manually by Solanki (1986). This confirms that the previously determined values are relatively reliable as far as uniqueness in the (ξ_{mac}, a_{mac}) plane is concerned. In particular, the code always gives a^V_{mac} close to zero, confirming the practice of setting $a^V_{mac}=0$ for all lines.

For the microturbulence inside the fluxtubes we have used two different μ dependences. First assuming $\xi^{fluxtube}_{mic}(\mu)=\xi^{fluxtube}_{mic}(\mu=1)=1$ km s^{-1}, later assuming $\xi^{fluxtube}_{mic}(\mu)=\xi^{quiet}_{mic}(\mu)$, where the quiet sun microturbulence has been taken from Simmons and Blackwell (1982). We have computed ξ^V_{mac} for each of the 11 selected lines at all 9 limb positions, but we have not obtained acceptable fits and at the same time reasonable values for ξ^V_{mac} for all lines and at all positions on the disk. The main culprit for the failure of the analysis in some cases is clearly the strong noise affecting the spectra, which makes it impossible to fit the weak lines with reasonable velocity broadenings. The strongly split lines Fe I 5247.1 Å and Fe I 5250.2 Å do not allow good fits either, since we have now increased the field strength in the models, so that $B(\tau=1)=2000$ G, in accordance with the line ratio results of Solanki et al. (1987). This means that the I_V profile is no longer a good approximation of Stokes I for these two lines, although it remains a good approximation of the unsplit I profile.

Figure 10 shows ξ^V_{mac} vs. μ for Fe II 5197.6 Å. The upper curve results when ξ_{mic} inside the fluxtube is assumed to be 1 km s^{-1} independent of μ. The lower curve results when $\xi_{mic}(\mu)$ inside the fluxtube is chosen to be the same as outside. As expected the slope of the linear regression has decreased. For reasons which have been discussed by Solanki (1986) this decrease is greater than what one would expect if the total turbulence velocity $\sqrt{(\xi^V_{mac}(\mu))^2+(\xi_{mic}(\mu))^2}$ were conserved. The estimated error is about 0.20–0.30 km s^{-1}. The Fe I lines for which reliable $\xi_{mac}(\mu)$ have been obtained, give rise to similar curves with approximately

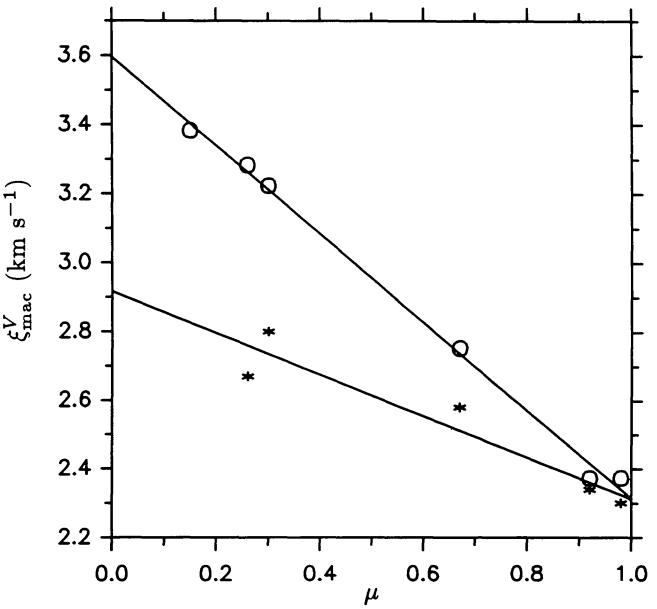

Fig. 10. CLV of the macroturbulence velocity inside the fluxtubes, ξ^V_{mac}, as derived from a fit to the full I_V profile of the Fe II 5197.6 Å line. The circles and upper straight line represent the macroturbulence if $\xi_{mic}=1$ km s^{-1} at all μ inside the fluxtube, while the stars and the lower straight line correspond to the macroturbulence derived for $\xi^{fluxtube}_{mic}(\mu)=\xi^{quiet}_{mic}(\mu)$

the same slopes but generally somewhat smaller velocities. We find that although the I_V profile shape can be reproduced quite well near disk centre, the fits become quite poor at $0.45 \lesssim \mu \lesssim 0.67$ (the observed I_V profiles are much more U shaped than the calculated I profiles). We have therefore not plotted the ξ^V_{mac} deduced from such regions. This observation is in agreement with what was noted by Solanki et al. (1987) when attempting to reproduce the V profile. The probable reason for the mismatch between observations and theory when considering line shapes is due to effects arising from the neglect of the finite width of fluxtubes.

If we plot ξ^V_{mac} vs. γ instead of μ, then the scatter is somewhat larger, but the main result is not affected, i.e., the velocity does not decrease with increasing γ.

We have also carried out a more comprehensive statistical analysis of a large number of lines which permits the dependence of macroturbulence on line strength to be investigated as well. Small differences in the physical properties of the observed regions (filling factor, temperature, average orientation of the magnetic field, etc.) may not always be completely compatible with the chosen standard atmosphere, making perfect fits to all three line parameters $\ln(d_V/d_I)$, v_{D_V}, $v_{D_V}-v_{D_I}$ often rather difficult (see Figs. 9, 12a, b). Of course this problem exists with the few-lines analysis as well. The main advantage of the many-lines approach is that it is less susceptible to noise in the individual profiles, so that we can determine ξ^V_{mac} for the weaker lines as well. Figure 11 shows the macroturbulence as a function of S_I which we have obtained by fitting the line widths as well as possible. In this case we have once more assumed $\xi^{fluxtube}_{mic}(\mu)=\xi^{quite}_{mic}(\mu)$. Since the curves for the regions with $\mu \lesssim 0.4$ on the one hand (solid), and the curves for $\mu \gtrsim 0.6$ on the other hand (dashed) lie close to each other, so that differences within each group are not significant, we have

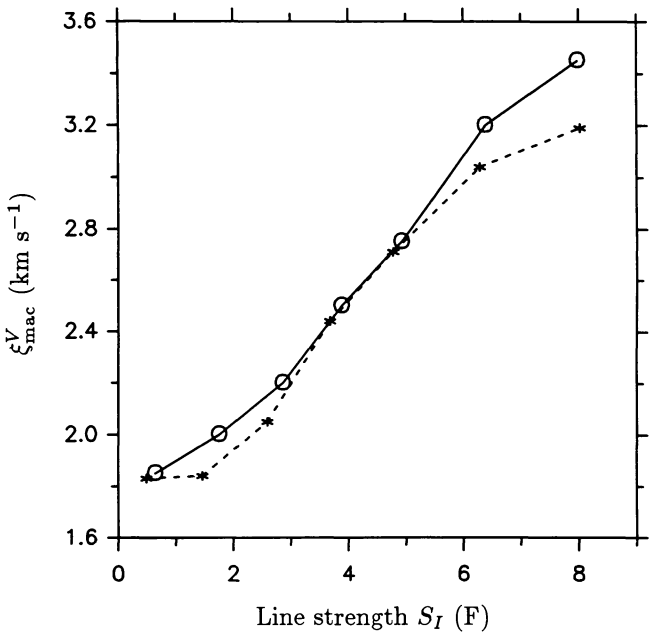

Fig. 11. ξ^V_{mac} vs. S_I as derived from the $v_{D_V}-v_{D_I}$ vs. S_I and v_{D_V} vs. S_I scatter plots of many Fe I lines and model calculations of $\chi_e = 3$ eV lines. Stars and dashed curve represent ξ^V_{mac} for regions with $\mu > 0.6$, while the open circles and the solid curve represent ξ^V_{mac} for regions with $\mu \leq 0.3$

reproduced only the average curves for the two sets. (Note that only the regions at $\mu = 0.30$ and $\mu = 0.28$ have been used for $\mu \leq 0.4$, since only for these regions do we have quiet sun spectra for comparison.) As a consequence of the uncertainty of approximately 0.30 km s^{-1}, the two curves can be regarded as indistinguishable for $S_I \lesssim 4.5$ F. It is unclear as to how significant the difference is for the stronger lines, although the strong lines fitted individually as described above also show a similar increase in ξ^V_{mac} with decreasing μ. If we recall that the asymmetry of Stokes V also changes near $\mu = 0.4$, then it may be that there is an associated physical change in the observed velocity structure at this μ. A striking feature of Fig. 11 is the strong dependence of ξ^V_{mac} on line strength, which is considerably stronger than that of ξ^I_{mac} derived by fitting quiet sun with synthetic profiles calculated in the HSRASP atmosphere (see Fig. 5a of Solanki, 1986).

How well such velocity broadened models reproduce the line width data is indicated in Fig. 12. Figure 12a shows v_{D_V} for a plage region observed at $\mu = 0.28$ and for lines calculated with the plage temperature model. The lower curve (dashed) represents model calculations without any velocity broadening, while the upper curve (solid) is obtained when broadening the lines to match the data. Since we have previously always considered only th $v_{D_V}-v_{D_I}$ vs. S_I diagram, we plot the data and models in this form as well. As can be seen from Fig. 12b, the same velocities that reproduce v_{D_V} alone also suffice for $v_{D_V}-v_{D_I}$, although slightly higher values (by approximately 0.2–0.3 km s^{-1}) may be required to obtain a more perfect fit. Note that in contrast to disk centre, where $v_{D_V} \approx v_{D_I}$ for almost all the lines plotted, near the limb v_{D_V} is smaller than v_{D_I} by approximately 0.5 km s^{-1} for the weaker lines, while the I_V profiles of the stronger lines can be both broader or narrower than their Stokes I profiles, depending on their excitation potential.

5. Discussion

In the present paper we have investigated a sample of FTS spectra of Stokes I and V obtained at various distances from the solar limb. We have broadly followed the statistical approach used previously by Solanki and Stenflo (1984, 1985) and Solanki (1986) on data obtained near disk centre.

We find that the Stokes V amplitude asymmetry decreases towards the limb, while the area asymmetry changes sign. The observations of δA which we have presented here can give us some indication of which mechanisms may be responsible for producing the asymmetry. Stokes V of the weakest lines should exhibit no area asymmetry if velocity gradients are the cause. This is not necessarily the case if it is caused by atomic orientation requiring departures from an LTE population of the magnetic substates. The weakest Fe I lines in the nine regions considered by us do appear to have a non-vanishing δA, although the noise is considerable. In any case this indication provides an incentive to observe Stokes V profiles of very weak lines with an extremely high S/N ratio.

The observation that δA changes sign near the limb can be easily explained in a qualitative manner in terms of velocity gradients (see e.g. Auer and Heasley, 1978), in particular as we probably have a complicated velocity field in and around the fluxtubes. If we take the finite thickness of fluxtubes into account, then velocities outside them, e.g. from the surrounding granules, may also influence the Stokes V profile shape. Atomic orientation, on the other hand, appears at first sight not to be able to account for this change in sign. Imagine that the iron atoms inside the fluxtube are oriented preferably in a vertical direction throughout the photospheric layers, such that when looking straight down the fluxtube (i.e. observing at disk centre) the blue wing of Stokes V is stronger than the red wing. If instead we were to observe the same system at an angle θ to the vertical (i.e. near the limb), then we would expect the asymmetry to be smaller, but to retain its sign.

However, the observations can be at least qualitatively explained if we assume a two layered model of atomic orientation. A lower atmosphere layer in which the atoms are oriented such that the V profiles formed in that layer have blue area greater than red area, while in a higher atmospheric layer the atoms have the opposite preferred orientation. Thus near disk centre the weak and medium strong lines would be formed in the lower layer, while the strongest lines would be formed close to the boundary between the two layers. Then δA would tend to decrease with line strength for the medium strong and strong lines, as observed. As we move towards the limb the lines are formed higher up, so that first the strong lines, and later increasingly weaker lines are formed in the second layer, which causes the asymmetry to change sign. Qualitatively, this behavior corresponds to the results of Sect. 3.2. One should keep in mind that this simple model does *not* explain how two such layers of oppositely oriented atoms can be produced, which appears to us to be much more difficult to explain.

Thus, the observations cannot yet completely rule out either of the two basic mechanisms so far invoked to explain the Stokes V area asymmetry, although gradients of *stationary* flows do not seem to be able to account for the observations.

The fact that the Stokes V asymmetry has a larger absolute value near the limb than near disk centre suggests that *if* it is produced by velocity gradients, then horizontal velocity gradients must be larger than vertical velocity gradients. This inference is

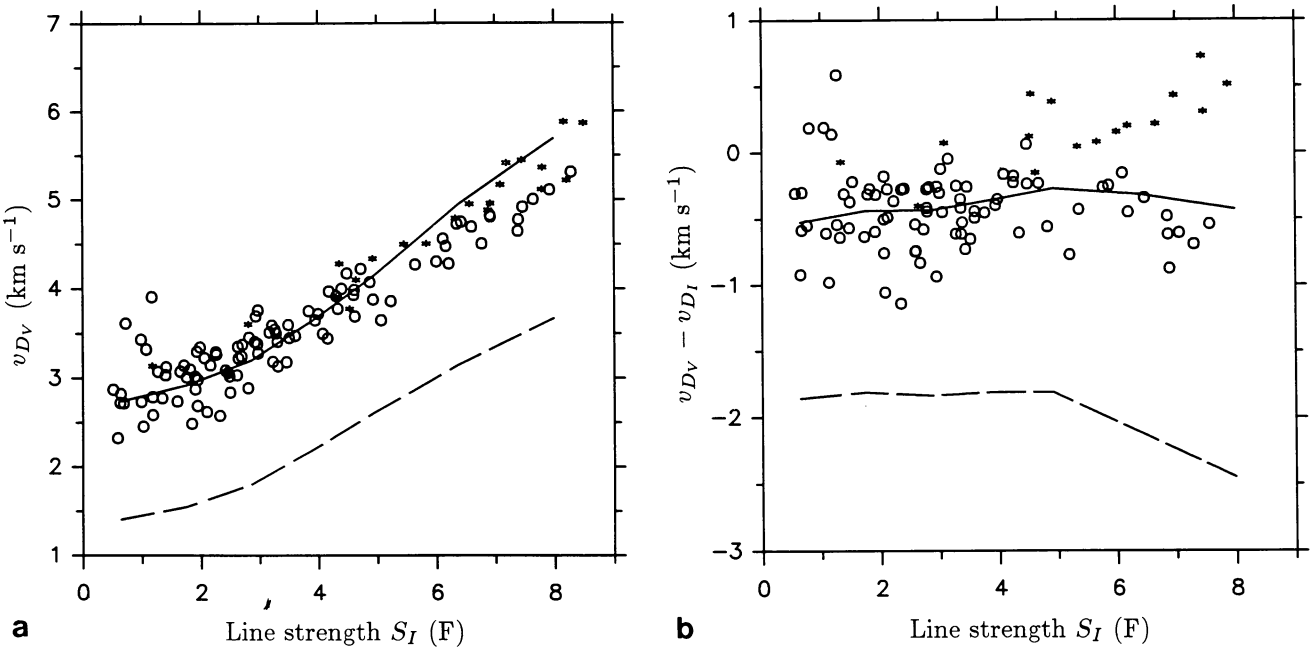

Fig. 12. **a** v_{D_V} vs. S_I. Comparison of model calculations (plage temperature model) with data obtained at $\mu = 0.28$. Lower curve (dashed) is calculated for lines without any velocity broadening. Upper curve (solid): Lines broadened with ξ^V_{mac} shown in Fig. 11 (solid curve in that figure). **b** Same as **a**, except that $v_{D_V} - v_{D_I}$ is given vs. S_I

supported by the large horizontal velocities which we have derived from the line widths, and by the current theoretical picture of magnetic fluxtubes, which are thought to be bounded by a thin current sheet. These strong area asymmetries may therefore be telling us something about the structure of the fluxtube walls. However, their interpretation is very involved. Another possibility is that since the spectral lines in the fluxtubes are strengthened considerably near the limb as compared with the disk centre (cf. Sect. 4.2), they are also more asymmetric, since in the model the asymmetry is not only a result of the combination of velocity and magnetic field gradients, but of line saturation as well.

In general agreement with the results of Stenflo and Harvey (1985), Solanki (1986), and Stenflo et al. (1987) we find that the CLV of the Stokes V zero-crossing shifts is compatible with an absence of significant stationary flows. There appears to be a tendency for the strong lines to be more blueshifted than the weak ones (in accordance with the disk centre results of Solanki, 1986).

Our regression analysis has confirmed that a dependence of fluxtube temperature on filling factor α exists, with regions having a larger α usually possessing fluxtubes with lower temperature than regions with smaller α. In addition to this temperature dependence on α, the data show a strong dependence on limb position μ. Both the α and μ dependence are approximately reproduced by the fluxtube models of Solanki (1986), which also give reasonable, if not quite perfect, fits to $\ln(d_V/d_I)$ vs. S_I and to the v_{D_V} vs. S_I (and $v_{D_V} - v_{D_I}$ vs. S_I) diagrams simultaneously near the limb as well as at disk centre. We find that the average $T(\tau)$ in the fluxtubes in most of the analysed regions lies within the range covered by the plage and network models. These models have also been shown to approximately reproduce the CLV of the Stokes Q σ–π asymmetry of two lines by Solanki et al. (1987). We consider the comparison with the data of the present paper to be the more stringent test.

We wish to caution, however, that possibly the true temperature structures in fluxtubes are quite different from those of the models mentioned above (or of any other empirical fluxtube models published so far). There are two main reasons for this caveat: The models are based on purely LTE calculations, and Solanki and Steenbock (1987) have demonstrated that the fluxtube temperature can be considerably changed if NLTE effects are taken into account in the empirical modelling (see also Rutten and Kostik, 1982). Furthermore the models considered here are based on the assumption of a plane parallel fluxtube atmosphere. Van Ballegooijen (1985) has illustrated the importance of fluxtube geometry, while 1.5-D calculations (i.e. calculations involving many parallel lines of sight) by Solanki and De Martino (unpublished) have shown that empirical 1-D (i.e. plane parallel) model calculations can underestimate the fluxtube temperature considerably.

Finally, let us discuss the possible sources of the large line broadening of the I_V profiles near the solar limb. We observe that instead of decreasing towards the limb, as expected if the broadening were due to mass motions parallel to the field lines, the rms velocity amplitude actually increases. A number of possible explanations come to mind. One possibility is that the broadening near the limb is not due to velocity at all. The obvious candidates in this case, thermal and magnetic broadening, can be ruled out. It is not possible to reproduce the decrease in line depth inside the fluxtube, while making the lines sufficiently wide just through thermal broadening. Harvey et al. (1972) have previously noted that the measured V profiles of Fe I 5250.2 Å are broader than the calculated ones. They had to artificially broaden the calculated profiles to make them match the data. They interpreted this broadening as due to a spread in the magnetic field strength. Indeed for only one V profile, it is not possible to distinguish between broadening due to velocity or to a magnetic field.

However, with many lines of various $g_{\rm eff}$ we can test the two hypotheses. Most of the lines in our sample have Landé factors near unity and are therefore not particularly sensitive to magnetic broadening, so that the non-thermal broadening must be mainly due to velocity.

The very high spectral resolution of the FTS rules out instrumental spectral broadening as a possible source. Another possibility is that the finite entrance aperture width of the FTS samples areas on the sun with somewhat different μ and therefore different solar rotation values. This leads to an increase in line width. A related effect results from the relatively long integration times. During integration the Earth has rotated somewhat and the entrance hole has shifted on the solar disk as well (since we tracked the observed regions using the law of differential rotation of solar magnetic fields). The combined line broadening resulting from these two effects is estimated to be less than 100 m s^{-1} even in the most pessimistic case closest to the limb. Note that $v_{D_V}-v_{D_I}$ is independent of this effect anyway, and this parameter also gives large velocities.

We are left with a number of solar sources. One possibility is that motions from outside the fluxtubes also broaden the lines. Although such motions can give rise to Stokes V asymmetry, it is not clear how they can *broaden* V profiles sufficiently, in particular since the velocities inside the fluxtubes are found to be higher than those outside. Since the five minute oscillations have not been measured in Stokes V away from disk centre we have no knowledge of their amplitudes, but we do not expect these to be larger than at disk centre, i.e. 0.25 km s^{-1}, a value which is completely inadequate to explain the observed line widths. Consequently we believe that the major part of the line broadening of the I_V profiles is caused by a combination of various wave modes and by the granulation induced jiggling of fluxtubes.

The following wave modes are possible candidates: transverse (i.e. kink and higher order modes), torsional (Alfvén) and longitudinal (sausage). Longitudinal waves are also expected to give a transverse signal since fluxtubes are not rigid, although the transverse signal probably has a much smaller amplitude than the longitudinal signal. The various wave modes in slender fluxtubes have been recently reviewed by Thomas (1985) and Roberts (1986). Longitudinal waves can be excited by a compression of the fluxtube through e.g. the downwards flow of material in the surrounding granulation. Transverse waves are associated with a bulge in a given direction. They can be excited by the jiggling of fluxtubes due to the surrounding granulation. This jiggling can itself give rise to a line broadening. Its magnitude is estimated by Parker (1983, 1986) to be of the order of 0.5–1 km s^{-1}. He invokes it as one of the basic mechanisms for heating the upper solar atmosphere when combined with reconnection. Finally, Alfvén waves (e.g. Parker, 1979) are also a possible source. These torsional waves can be excited by a whirl flow in the surroundings, which in turn is due to the bathtub effect in a localised downflow in the fluxtube surroundings (Nordlund, 1983; Schüssler, 1984).

Observational evidence for transverse wavelike motions in the chromospheric parts of fluxtubes has been presented by Giovanelli (1975), from time series of photographs of H_α fibrils at supergranule boundaries and in active regions.

Acknowledgements. We are greatly indebted to P.N. Brandt for allowing us to use one of his quiet sun spectra prior to publication. Discussions with U. Grossmann-Doerth on Stokes V asymmetry mechanisms are gratefully acknowledged. The work of one of us (S.K.S.) has been partially supported by grant No. 2.666-0.85 of the Swiss National Science Foundation.

References

Auer, L.H., Heasley, J.N.: 1978, *Astron. Astrophys.* **64**, 67
Beckers, J.M.: 1969a, *Solar Phys.* **9**, 372
Beckers, J.M.: 1969b, *Solar Phys.* **10**, 262
Brault, J.W., White, O.R.: 1971, *Astron. Astrophys.* **13**, 169
Caccin, B., Falciani, R., Donati-Falchi, A.: 1976, *Solar Phys.* **46**, 29
Chapman, G.A.: 1979, *Astrophys. J.* **232**, 923
Gingerich, O., Noyes, R.W., Kalkofen, W., Cuny, Y.: 1971, *Solar Phys.* **18**, 347
Giovanelli, R.G.: 1975, *Solar Phys.* **44**, 299
Gopasyuk, S.I., Kotov, V.A., Severny, A.B., Tsap, T.T.: 1973, *Solar Phys.* **31**, 307
Grossmann-Dœrth, U., Pahlke, K.-D., Schüssler, M.: 1987, *Astron. Astrophys.* **176**, 139
Harvey, J.W., Livingston, W., Slaughter, C.: 1972, in *Line Formation in the Presence of Magnetic Fields*, High Altitude Obs., NCAR, Boulder, CO, p. 227
Holweger, H.: 1979, in *Proc. 22nd Liège International Astrophys. Symp.*, Inst. d'Astrophysique, Liège, p. 117
Holweger, H., Gehlsen, M., Ruland, F.: 1978, *Astron. Astrophys.* **70**, 537
Howard, R.W., Stenflo, J.O.: 1972, *Solar Phys.* **22**, 402
Illing, R.M.E., Landman, D.A., Mickey, D.L.: 1974, *Astron. Astrophys.* **35**, 327
Illing, R.M.E., Landman, D.A., Mickey, D.L.: 1975, *Astron. Astrophys.* **41**, 183
Kemp, J.C., Macek, J.H., Nehring, F.W.: 1984, *Astrophys. J.* **278**, 863
Livingston, W.C.: 1983, in J.O. Stenflo, ed., *Solar and Stellar Magnetic Fields: Origins and Coronal Effects*, IAU Symp. **102**, p. 149
Mihalas, D.: 1978, *Stellar Atmospheres*, Freeman and Company, San Francisco
Nordlund, Å.: 1983, in J.O. Stenflo, ed., *Solar and Stellar Magnetic Fields: Origins and Coronal Effects*, IAU Symp. **102**, p. 79
Parker, E.N.: 1979, *Cosmical Magnetic Fields*, Clarendon Press, Oxford
Parker, E.N.: 1983, *Astrophys. J.* **264**, 642
Parker, E.N.: 1986, in W. Deinzer, M. Knölker, H.H. Voigt, eds., *Small Scale Magnetic Flux Concentrations in the Solar Photosphere*, Vandenhoeck and Ruprecht, Göttingen, p. 13
Roberts, B.: 1986, in W. Deinzer, M. Knölker, H.H. Voigt, eds., *Small Scale Magnetic Flux Concentrations in the Solar Photosphere*, Vandenhoeck and Ruprecht, Göttingen, p. 169
Rutten, R.J., Kostik, R.I.: 1982, *Astron. Astrophys.* **115**, 104
Schüssler, M.: 1984, *Astron. Astrophys.* **140**, 453
Schüssler, M., Solanki, S.K.: 1987, *Astron. Astrophys.* (in press)
Simmons, G.J., Blackwell, D.E.: 1982, *Astron. Astrophys.* **112**, 209
Solanki, S.K.: 1986, *Astron. Astrophys.* **168**, 311
Solanki, S.K.: 1987a, in *Proc. Workshop on The Role of Fine-Scale Magnetic Fields on the Structure of the Solar Atmosphere*, Tenerife, 6–12 Oct. 1986 (in press)
Solanki, S.K.: 1987b, *Ph.D. Thesis*, ETH, Zürich
Solanki, S.K., Keller, C., Stenflo, J.O.: 1987, *Astron. Astrophys.* (in press)
Solanki, S.K., Steenbock, W.: 1987, *Astron. Astrophys.* (in press)
Solanki, S.K., Stenflo, J.O.: 1984, *Astron. Astrophys.* **140**, 185

Solanki, S.K., Stenflo, J.O.: 1985, *Astron. Astrophys.* **148**, 123
Spruit, H.C.: 1974, *Solar Phys.* **34**, 277
Stenflo, J.O., Harvey, J.W.: 1985, *Solar Phys.* **95**, 99
Stenflo, J.O., Harvey, J.W., Brault, J.W., Solanki, S.K.: 1984, *Astron. Astrophys.* **131**, 33
Stenflo, J.O., Lindegren, L.: 1977, *Astron. Astrophys.* **59**, 367
Stenflo, J.O., Solanki, S.K., Harvey, J.W.: 1987, *Astron. Astrophys.* **171**, 305
Thomas, J.H.: 1985, in H.U. Schmidt, ed., *Theoretical Problems in High Resolution Solar Physics*, Max Planck Inst. f. Astrophys., Munich, p. 126
Unsöld, A.: 1955, *Physik der Sternatmosphären*, Springer Verlag, Berlin, Heidelberg
Van Ballegooijen, A.A.: 1985, in M.J. Hagyard, ed., *Measurements of Solar Vector Magnetic Fields*, NASA Conf. Publ. 2374, p. 322